Mon. Not. R. Astron. Soc. **355,** 1031–1040 (2004) doi:10.1111/j.1365-2966.2004.08406.x

Comparison of the effective temperatures, gravities and helium abundances of DAO white dwarfs from Balmer and Lyman line studies

S. A. Good,[1⋆] M. A. Barstow,[1] J. B. Holberg,[2] D. K. Sing,[2] M. R. Burleigh[1] and P. D. Dobbie[1]

[1]*Department of Physics and Astronomy, University of Leicester, University Road, Leicester LE1 7RH*
[2]*Lunar and Planetary Laboratory, University of Arizona, Tucson AZ 85721, USA*

Accepted 2004 September 1. Received 2004 August 19; in original form 2004 May 18

ABSTRACT

The use of observations of the hydrogen Balmer absorption series is a well-established method of determining the surface gravity and effective temperature ($T_{\rm eff}$) of white dwarfs. In situations where the Balmer lines cannot be used it is possible to use the hydrogen Lyman series instead. However, previous studies by Barstow et al. have shown that for DAs (hydrogen-rich, no helium) hotter than ∼50 000 K the Lyman lines systematically yield higher values of $T_{\rm eff}$ than the Balmer lines. Analysis of optical and *FUSE* spectra of 16 DAO white dwarfs (hybrid hydrogen/helium) demonstrates that temperatures measured using the different data sets continue to diverge at even higher temperatures, and in three extreme cases $T_{\rm eff}$ derived from the Lyman lines is in excess of 120 000 K. These discrepancies are observed to decrease at lower gravities and luminosities. Helium abundances were also determined from the strength of He II lines in the two wavelength regimes. These agree well, even though the temperatures differ considerably, with the exception of two DAO+M dwarf binaries. For these, the change in the measured helium abundance may result from the different times at which the objects were observed in the two wavelength regimes.

Key words: stars: atmospheres – white dwarfs – ultraviolet: stars.

1 INTRODUCTION

Knowledge of the effective temperature ($T_{\rm eff}$) and surface gravity of a white dwarf is vital to our understanding of its evolutionary status. It is possible to obtain unique values for both parameters by comparing the profiles of the hydrogen Balmer lines that are seen in optical observations to theoretical models. This technique was pioneered by Holberg et al. (1985) and extended to a large sample of white dwarfs by Bergeron, Saffer, & Liebert (1992). It is now the standard method for studying isolated white dwarfs that are hotter than ∼15 000 K, for which complications associated with convection are much reduced, and can also be used for stars cooler than ∼10 000 K that are outside the ZZ Ceti range. However, for objects in close binary systems, where the white dwarf cannot be spatially resolved, the Balmer line profiles are frequently contaminated by flux from the secondary (if it is of type K or earlier) and they cannot be used to determine $T_{\rm eff}$ and log g. A similar technique can instead be applied to the Lyman lines that are found in far-ultraviolet (far-UV) data, as the white dwarf is much brighter in this wavelength region than the companion (e.g. Barstow et al. 1994b). If we are to rely on the results from the two wavelength regions, it is important that the $T_{\rm eff}$ and log g they yield should be consistent. An initial investigation of this was conducted by Barstow et al. (2001b). They analysed data from the *Hopkins Ultraviolet Telescope* (*HUT*), the *Orbiting and Retrievable Far and Extreme Ultraviolet Spectrometers* (*ORFEUS*) and the *Far Ultraviolet Spectroscopic Explorer* (*FUSE*) observatories, each of which are sensitive to wavelengths that cover more than one Lyman line (the requirement for obtaining unambiguous measurements of $T_{\rm eff}$ and log g) and compared the results to those obtained from Balmer line studies. In general, good agreement was found between the two wavelength regions, although there were significant differences in some cases. In these instances, the measurements from one wavelength region were not systematically greater than measurements from the other, which would be expected if the differences were related to limitations in the stellar models. Instead it was concluded that systematic effects arising from observations, data reduction and analysis were causing the discrepancies. However, the study was limited in the main to objects that were cooler than 50 000 K.

Subsequently, Barstow et al. (2003b) used an expanded data set of 16 white dwarfs from the extensive *FUSE* archive to extend the temperature range of the sample upwards. They found that above 50 000 K the results started to diverge, with the Lyman lines systematically giving a higher temperature than a fit to the Balmer lines of the same object. It was not clear if it was the Lyman or the Balmer lines, or neither, that were giving the correct results, although it was possible to find an empirical relationship between the Balmer and

⋆E-mail: sag@star.le.ac.uk

Lyman $T_{\rm eff}$ values. Two objects did not fit into this relationship; the Lyman $T_{\rm eff}$ for RE 0457−281 was larger than the Balmer measurement at a level significantly higher than for the other objects, while conversely PG 1342+44 was the only object whose Lyman $T_{\rm eff}$ was significantly lower than that obtained from the Balmer lines. The measurements of log g agreed with each other well, apart from for four outlying objects. Two of these had log g above 7.8, but the others had the lowest gravities in the sample. The measurement disagreements in the high-gravity objects may have been caused by their unusual nature; GD 394 is photometrically variable in the extreme UV (EUV), and may experience episodic accretion, while WD 1620−391 shows quasi-molecular Lyman satellite lines, which were not included in the model atmosphere calculations. The two low-gravity objects might represent a true departure from equal Balmer and Lyman log g measurements towards low gravity, although this could not be confirmed without including more low-gravity objects in the sample. Use of *FUSE* data had the additional advantage that multiple observations of some of the objects could be used to measure the uncertainty in the measurements. This demonstrated that the formal errors underestimate the true uncertainties by a factor of 2–3.

The studies by Barstow et al. (2001b) and Barstow et al. (2003b) looked at DAs, whose optical spectra contain hydrogen Balmer lines only. The hottest star in their sample (REJ1738+665) was measured to have a temperature of 66 760 ± 1230 K from Balmer line measurements and 75 799 ± 685 K from measurements of the Lyman lines. It is therefore of interest to perform a similar comparison for DAO white dwarfs, for which helium lines are visible in their optical spectra as well as hydrogen, and which generally have higher temperatures than the DAs, to see if the problem is present and at the same level. In addition, a large proportion of the DAOs are known to have low gravity and can be used to investigate the possible divergence observed by Barstow et al. (2003b) towards low log g values. Barstow et al. (2003b) concluded that it was likely to be the detailed physics that is input into the models that is source of the problem, so the different conditions found in DAOs, for example the enhanced helium found in their line-forming regions, and their different evolutionary paths might give some further insight into the problem.

DAO white dwarfs, for which the prototype is HZ 34 (Koester, Weidemann & Schulz 1979; Wesemael et al. 1993), are observed to have He II lines in their optical spectra in addition to the strong hydrogen Balmer features. As radiative forces are unable to support sufficient helium to reproduce these lines (Vennes et al. 1988), one explanation for the existence of these stars is that they are transitional objects switching between the helium- and hydrogen-rich cooling sequences. This could happen if a small amount of hydrogen were mixed into an otherwise helium-dominated atmosphere. Gravitational settling would then create a thin hydrogen layer at the surface of the white dwarf, with the boundary between the hydrogen and helium described by diffusive equilibrium. However, Napiwotzki & Schöberner (1993) attempted to reproduce the line profile of the He II line at 4686 Å in the DAO S 216 using both stratified and homogeneous composition models and found that a better match was provided by the latter. Subsequently, a spectroscopic investigation of a large sample of DAOs by Bergeron et al. (1994) found that the He II line profile of only one out of a total of 14 objects was better reproduced by stratified models. In addition, the line profile of a second (PG 1210+533) could not be reproduced satisfactorily by either set of models. This object is known to be unusual because the line strengths of its helium lines have been observed to change over a time period of ∼15 yr (Bergeron et al. 1994).

Most of the remaining objects in the Bergeron et al. sample were comparatively hot for white dwarfs, but with low gravity, which implies they have low mass. Therefore, the progenitors of some of these DAOs are unlikely to have had sufficient mass to ascend the asymptotic giant branch (AGB), and instead they may have evolved from the AGB-manqué stars, which, after core helium exhaustion, cannot evolve onto the AGB as their hydrogen envelope mass is insufficient. Bergeron et al. (1994) suggested that weak mass loss may be occurring in these stars, which could act against gravitational settling and might support the observed quantities of helium in the line-forming regions of the DAOs (Unglaub & Bues 1998, 2000). Three objects (RE 1016−053, PG 1413+015 and RE 2013+400) had 'normal' temperatures and gravities, yet still had detectable helium lines in their optical spectra. These three stars are all close binary systems containing M dwarf (dM) companions. Two reasons were suggested for this: first, as the progenitor star passes through the common envelope phase, mass will be lost. This may lead to the star being hydrogen poor, allowing a weak process, such as mass loss, to mix helium into the line-forming region of the white dwarf. Secondly, these DAOs might be accreting from the wind of their companions. This seems the most likely explanation for a fourth DAO+dM binary, RE 0720−318, which was not included in the sample of Bergeron et al. (1994). Dobbie et al. (1999) used EUV photometry and phase-resolved spectroscopy to identify likely non-uniformities in the surface abundance of helium, which is consistent with models of accretion.

A well-known problem with the use of the Balmer lines to determine the $T_{\rm eff}$ and log g of white dwarfs and subdwarfs is the so-called 'Balmer line problem'. For some stars the higher order Balmer lines (e.g. δ and ϵ) require a higher temperature model to fit their profiles than the lower order (e.g. β and γ) lines (Napiwotzki & Schöberner 1993). By comparing objects with similar parameters but where different strengths of the effect were seen, Bergeron et al. (1994) were able to exclude $T_{\rm eff}$ and log g effects as the cause of the problem. Nor does it appear confined to the DAOs; a footnote added in proof to Bergeron et al. (1994) states that they found a hot DA (PG 0948+534) that exhibited the problem. Werner (1996) found that the effect could be accounted for in an sdO star by including the Stark broadening of C, N and O in their models. If this is the case, the higher order Balmer lines should be least affected by this omission and should yield a value closest to the 'correct' temperature (Napiwotzki 1999). However, in their analysis of WD 2218+706, which had previously been identified as exhibiting the effect by Napiwotzki (1999), Barstow et al. (2001a) found that a statistically acceptable fit could be obtained when fitting the $\beta - \delta$ Balmer lines simultaneously to give a consistent temperature for all the lines, although a better fit was obtained if, for each line, the temperature of the model was allowed to vary independently. They noted that many hot DAs do not exhibit the problem, and that it tends to be associated with stars surrounded by a planetary nebula, calling into question the above explanation. As the single temperature fit could not be rejected on statistical grounds, but is more physical and self-consistent, they chose to use a single $T_{\rm eff}$ fit, and this is also the approach adopted for our analysis.

2 OBSERVATIONS

2.1 Balmer line spectra

A programme of spectroscopic observations of DAO white dwarfs was undertaken using the Steward Observatory 2.3-m Bok telescope on Kitt Peak, Arizona, USA during 2001, as part of a

follow-up programme to *FUSE* observations. These data, which cover wavelengths between 3846 and 4996 Å, have a resolution of ∼1–2 Å (FWHM), determined from the width of emission lines in the spectrum of HS 1136+6646. In addition, the data used by Bergeron et al. (1994) and the spectra of DeHt 5 (WD 2218+706) from Barstow et al. (2001a) are also reanalysed in this paper. The resolution of these differs from that of the newer data; for the Bergeron data the resolution is ∼8 Å (FWHM), while for the two spectra of DeHt 5, the values are 1.5 (FWHM) and 8 Å (FWHM). Measurement errors were estimated from the scatter in the data.

2.2 Lyman line spectra

Far-UV data for all the objects were obtained by the *FUSE* spectrographs and cover the full Lyman series, apart from Lyman α. Table 1 summarizes the observations, which were downloaded by us from the Multimission Archive (http://archive.stsci.edu/mast.html), hosted by the Space Telescope Science Institute. The *FUSE* satellite was launched on 1999 June 24 and placed into a low Earth orbit. After initial check-out and calibration activities, science operations began in December of the same year, hence approximately 4 yr of data have now been collected. Overviews of the mission and in-orbit performance have been published by Moos et al. (2000) and Sahnow et al. (2000) respectively, so the following is a brief summary of issues related to the use of the data.

The *FUSE* instrument consists of four separate co-aligned optical paths (channels). Each channel has a mirror, a focal plane assembly, a diffraction grating and part of a detector. Light from a target enters the apertures of all the channels at the same time. Two of the mirrors and two of the gratings are coated with LiF over a layer of aluminium, the others with SiC because the reflectivity of the Al+LiF is low below about 1020 Å. *FUSE* has two microchannel plate detectors (1 and 2), each divided into two segments (A and B) that are separated by a small gap. Light from a SiC and a LiF channel falls onto each detector. This results in eight individual spectra, which together provide wavelength coverage between 905 and 1187 Å. There are a number of different apertures available for use on *FUSE*, but as the target can move out of the aperture when thermal changes rotate the mirrors slightly, most observations have been carried out using the largest aperture (LWRS, 30×30 arcsec^2). In this aperture the spectral resolution has been found to be 20 000 for the LiF 1 channel (The *FUSE* observers guide – see http://fuse.pha.jhu.edu/), which is easily good enough to study the broad Lyman lines. *FUSE* has two modes for recording data – time-tagged event lists (TTAG data) or as spectral image histograms (HIST data), used where the source is bright. As *FUSE* is in a low-Earth orbit emission lines from the atmosphere of the Earth are sometimes seen. These lines are not removed in the data-reduction stage but instead are dealt with during the data analysis. A particular problem with *FUSE* spectra is the presence of the 'worm', which is a shadow cast by the electron repeller grid located above the detector surface, and manifests itself by a decrease in flux by up to 50 per cent, particularly in the LiF 1B segment. The amount of flux loss varies according to how closely the position of the grid wires coincides with the image, and is also affected by the position of the target in the aperture and so cannot easily be removed by the calibration software. This loss of flux is most noticeable away from the wavelength range of interest for this paper.

As a number of improvements have been made to the calibration pipeline since the data were originally processed and archived, after they were downloaded the data were reprocessed using a locally installed version of the CALFUSE pipeline [version 2.0.5 or later – Barstow et al. (2003b) found that the differences between these versions do not significantly affect the results of the fitting process]. Once processed by the CALFUSE pipeline the exposures for each segment are cross correlated, and a wavelength correction is calculated to account for drift between exposures. A co-added spectrum for each segment is then produced with each exposure weighted according to exposure time. If the target has drifted out of the aperture for any of the exposures then that exposure is not included. The spectrum for each segment is then inspected. The edges of the spectra are normally the noisiest and have the poorest wavelength solution,

Table 1. List of *FUSE* observations for the stars in the sample.

Object	WD number	Obs. ID	Date	Length (ks^{-1})	Aperture	TTAG/HIST
A 7	WD0500−156	B0520901000	2001/10/05	11.525	LWRS	TTAG
HS 0505+0112	WD0505+012	B0530301000	2001/01/02	7.303	LWRS	TTAG
PuWe 1	WD0615+556	B0520701000	2001/01/11	6.479	LWRS	TTAG
		S6012201000	2002/02/15	8.194	LWRS	TTAG
RE 0720−318	WD0718−316	B0510101000	2001/11/13	17.723	LWRS	TTAG
TON 320	WD0823+317	B0530201000	2001/02/21	9.378	LWRS	TTAG
PG 0834+500	WD0834+501	B0530401000	2001/11/04	8.434	LWRS	TTAG
A 31		B0521001000	2001/04/25	8.434	LWRS	TTAG
HS 1136+6646	WD1136+667	B0530801000	2001/01/12	6.217	LWRS	TTAG
		S6010601000	2001/01/29	7.879	LWRS	TTAG
Feige 55	WD1202+608	P1042105000	1999/12/29	19.638	MDRS	TTAG
		P1042101000	2000/02/26	13.763	MDRS	TTAG
		S6010101000	2002/01/28	10.486	LWRS	TTAG
		S6010102000	2002/03/31	11.907	LWRS	TTAG
		S6010103000	2002/04/01	11.957	LWRS	TTAG
		S6010104000	2002/04/01	12.019	LWRS	TTAG
PG 1210+533	WD1210+533	B0530601000	2001/01/13	4.731	LWRS	TTAG
LB 2	WD1214+267	B0530501000	2002/02/14	9.197	LWRS	TTAG
HZ 34	WD1253+378	B0530101000	2003/01/16	7.593	LWRS	TTAG
A 39		B0520301000	2001/07/26	6.879	LWRS	TTAG
RE 2013+400	WD2013+400	P2040401000	2000/11/10	11.483	LWRS	TTAG
DeHt 5	WD2218+706	A0341601000	2000/08/15	6.055	LWRS	TTAG
GD 561	WD2342+806	B0520401000	2001/09/08	5.365	LWRS	TTAG

so these are removed. If the worm is noticeable in a segment then the section of data with reduced flux is not used. Regions with strong photospheric lines in each segment are then cross correlated to find and correct for any wavelength shifts. Spectral fluxes are shifted by a constant factor to line up with the LiF 1A segment, which is the segment used in the pointing of the satellite and should have the best flux and wavelength calibrations. The segments are then co-added onto a single wavelength scale, typically with 0.02 Å binning, which oversamples the true resolution by ∼2.5 times. The data are weighted according to their signal-to-noise ratio, calculated over a running mean of 20 Å.

3 MODEL ATMOSPHERE CALCULATIONS

A grid of homogeneous model stellar atmospheres was calculated for this analysis using the non-local thermodynamic equilibrium (LTE) code TLUSTY (v. 198) (Hubeny & Lanz 1995) and its associated spectral synthesis program SYNSPEC (v. 46). Although there have since been newer versions of this software released that improve on and resolve issues with this combination of the programs, the changes made should not affect the white dwarf model atmospheres (Hubeny, private communication). However, to further ensure that the results obtained with these models are consistent with those from models calculated with different generations of the programs, test fits to optical and far-UV spectra were performed using grids of models that had previously been created, but could not not be used for studying all the DAOs in our sample because the parameter space covered was insufficient or because they did not include heavy elements. The results of these fits were found to be consistent with those obtained using the new grid.

All the data, including those from Bergeron et al. (1994) and Barstow et al. (2001b) are analysed with the same models to provide consistency between the Balmer and Lyman line measurements. The models are based on those used by Barstow et al. (2001b) and Barstow et al. (2003b), but as DAOs have measurable quantities of helium, grid points were calculated for a number of values of log He/H. The *FUSE* spectra of all the DAOs contain absorption lines owing to heavy elements. As the presence of these heavy elements can affect Balmer and Lyman line measurements (Barstow, Hubeny & Holberg 1998), they were included in the models at abundances determined in an earlier analysis of the hot DA white dwarf G 191−B2B with homogeneous models ($C/H = 4.0 \times 10^{-7}$, $N/H = 1.6 \times 10^{-7}$, $O/H = 9.6 \times 10^{-7}$, $Si/H = 3.0 \times 10^{-7}$, $Fe/H = 1.0 \times 10^{-5}$ and $Ni/H = 5.0 \times 10^{-7}$). The range of the grid of models was between 40 000 and 120 000 K with grid points every 10 000 K for $T_{\rm eff}$, while log g ranged between 6.5 and 8.0 in 0.5 steps, and log He/H between −5 and −1 in steps of 1.

4 MOLECULAR HYDROGEN MODELS

A number of the *FUSE* spectra contain molecular hydrogen absorption features. Grids of molecular hydrogen absorption models were created for rotational states 0 to 14 of the zeroth vibrational level of the ground electronic state using the templates of McCandliss (2003). Grid points were calculated for column densities up to a maximum 10^{21} cm^{-2} and Doppler parameters between 2 and 20 km s^{-1}. As the templates and hence the models take the form of multiplicative factors that represent the absorption owing to a rotational state at a certain wavelength, it is possible to combine multiple components together to simultaneously fit the line profiles of many rotational states.

5 DETERMINATION OF TEMPERATURE, GRAVITY AND HELIUM ABUNDANCE

The technique of comparing model predictions with observations of Balmer line profiles to determine $T_{\rm eff}$ and log g is well established (see Holberg et al. 1985; Bergeron et al. 1992). Our Balmer line analysis technique has been described in many earlier papers (e.g. Barstow et al. 1994a). As the objects in question are DAOs, the helium abundance is included as a free parameter within the fit, in addition to temperature and gravity. The fits to the hydrogen Lyman and helium lines in the *FUSE* data are very similar to those for the Balmer line data. For completeness, a summary of the technique is described again here. Illustrations of fits to the Balmer and Lyman line spectra for PG 1210+533 are shown in Figs 1 and 2 as examples of the results.

Analysis of both far-UV and optical data was conducted using the spectral fitting program XSPEC (Arnaud 1996), which uses a χ^2 minimization technique to determine the model spectrum that best matches the data. For the Balmer lines, Hβ through to Hϵ are simultaneously fitted. In addition, in this analysis, the helium abundance is measured, principally by fitting the profile of the He II line at 4686 Å, although in the cooler stars He I is also included, where detected. An independent normalization constant and, in poorer quality spectra, a slope correction, is applied to each to ensure that the result is independent of the local slope of the continuum and to reduce the effect of any systematic errors in the flux calibration of the spectrum.

As the Lyman lines overlap shortwards of Lyman β, the Lyman series is divided into two wavelength ranges: one containing the β line and the other γ through to ϵ. The helium abundance can also be measured by fitting the profile of a He II feature, the centre of which is at ∼1085 Å. Unfortunately, this wavelength region is covered only by the SiC 1A and 2B segments and partly by the very edge of LiF 2A. Consequently the data are noisy and the wavelength calibration might be uncertain in this area of the spectra. The flux calibration that was performed as part of the standard pipeline was assumed to be reliable and the same normalization constant was applied to each section of data. As a number of the FUSE spectra show features owing to molecular hydrogen, interstellar extinction might also be expected, which would modify the slope of the white dwarf spectrum and could influence the fits. To correct for this, the extinction model of Seaton (1979) was included in the fit.

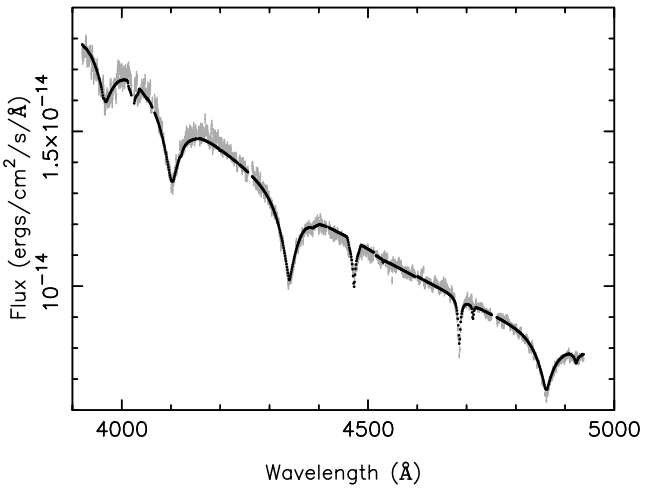

Figure 1. Example of a fit to Balmer lines, for PG 1210+533 (data, grey error bars; model, black dots).

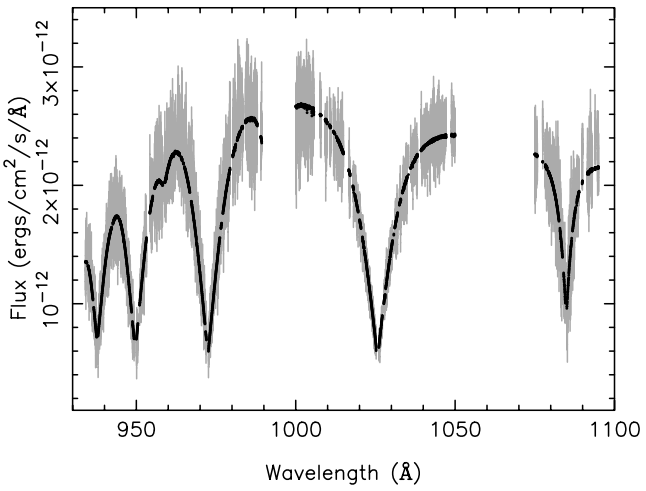

Figure 2. Example of a fit to *FUSE* data, for PG 1210+533 (data, grey error bars; model, black dots). To analyse the white dwarf spectrum, an interstellar extinction model is included in the fit. Strong photospheric or interstellar heavy element lines have been removed in order to prevent them influencing the fit.

Analysis of the Balmer lines is usually straightforward as, in general, they are uncontaminated by other components. The exception is where the star is part of a binary and the spectrum is a composite. In some cases a reflection effect, owing to reprocessing of the white dwarf flux on the surface of the white dwarf, may be seen and could bias the results of the Balmer line fits. The Lyman lines are often contaminated by strong emission lines, owing to the geocorona of the Earth, superimposed on the white dwarf spectrum. In addition, interstellar H I absorption may deepen the cores of the Lyman lines. Therefore, the centres of the Lyman lines, and other regions affected by airglow are excluded from the fits. All other interstellar features are also removed from the fit.

All of the *FUSE* spectra analysed here contain absorption features owing to heavy elements. In principle, it is possible to create models that they contain heavy elements with abundances that would reproduce these features. However, as the *FUSE* spectral range is only now becoming well studied, it is not certain that, in the context of white dwarf atmospheres, all possible transitions have been taken account of in the models and we have little experience of the reliability of the atomic data used. In addition, the detailed line profiles can be strongly affected by stratification of material in the atmospheres of the white dwarfs (see Barstow et al. 2003a), an effect that is not well understood. Evidence from recent work (e.g. Barstow et al. 1998) suggests that these details only have a secondary influence on the shape of the Balmer and Lyman lines. Therefore, we include heavy elements in our models at the same abundances that were measured for the well-studied DA G191−B2B, but we do not create individually tailored models for each star. If the strength of the heavy element absorption lines are not well reproduced by the models, for example because of the assumed homogeneous chemical structure of the atmosphere, the fit to the Balmer and Lyman lines will be affected. Consequently, all significant photospheric lines are removed from the spectrum during the analysis.

A number of the *FUSE* spectra are affected by molecular hydrogen absorption. If the H_2 column density is high, these features can be strong and broad, and can affect the shape of the Lyman lines. To account for this absorption, allowing the white dwarf spectrum to be analysed, the H_2 line profiles in wavelength regions longward of the broad Lyman features were fitted to the grids of H_2 models using XSPEC. The column density of each rotational level was allowed to vary independently of the others. At the signal-to-noise ratio of the *FUSE* observations, it was possible to detect column densities down to $\sim 10^{14}$ cm^{-2}. In most cases the Doppler parameter was allowed to vary, but was kept the same for each line. However, for a few objects extra components with a different Doppler parameter were required to achieve a satisfactory fit. Rotational levels were added until no significant improvement in the χ^2 fit statistic was achieved. Once the molecular hydrogen absorption for a star had been parametrized, a model was created using these values. This reproduced the H_2 features in the spectrum, allowing the white dwarf spectrum itself to be fitted (Fig. 3).

Table 2 lists the best-fitting parameters for each of the objects derived from fitting homogeneous models to the optical and *FUSE* data. As some of the objects have multiple observations, the results and their errors are averaged. The errors are the formal statistical uncertainties determined from the $\Delta\chi^2$ distribution corresponding to 1σ for 3 degrees of freedom. However, as the measurements of H_2 absorption have errors associated with them, which are not accounted for in the calculation of the formal errors, these uncertainties will be underestimated. In addition, these errors do not take into account the possible systematic effects related to the data calibration, reduction and analysis, which can outweigh the statistical uncertainties by a factor of 2–3 (Barstow et al. 2003b).

6 DISCUSSION

6.1 Effective temperature comparisons

Fig. 4 shows a scatter plot of the mean values of $T_{\rm eff}$ that were measured from Balmer and Lyman line data. The results show a continuation to higher temperatures of the empirical relationship between $T_{\rm eff}$ measured using Lyman and Balmer line studies that was found by Barstow et al. (2003b). To illustrate the disparity between the best-fitting models to the Balmer and to the Lyman lines, Fig. 5 shows an optical and *FUSE* spectrum of Ton 320, with the models overlaid. Although there is considerably more scatter

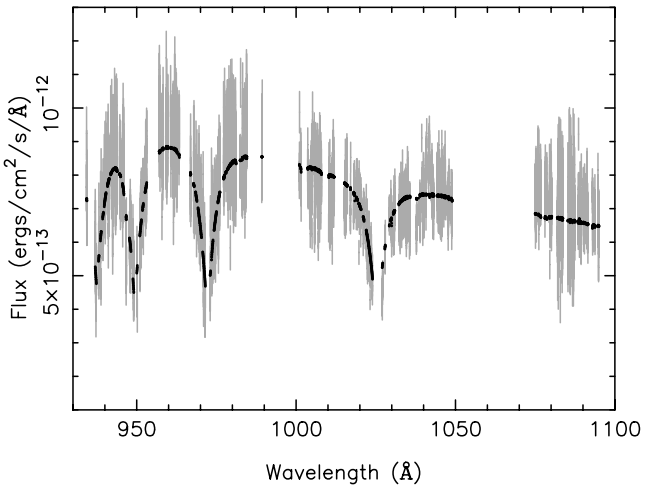

Figure 3. Example of a fit to *FUSE* data, for PG 0834+500 (data, grey error bars; model, black dots). For this star, a molecular hydrogen absorption model has been included in the fit in order to allow the white dwarf spectrum to be analysed. In addition, any narrow H_2 lines have been excluded from the fit to prevent small disagreements between the H_2 model and the detailed line profile biasing the fit to the white dwarf spectrum. This Lyman lines of this object are very weak compared to, for example, those of PG 1210+533 (Fig. 2), and the model shown has a temperature of 120 000 K.

Table 2. Mean best-fitting parameters obtained from optical and *FUSE* data. Log He/H is not listed for the optical data of PG 1210+533 as it is seen to vary between observations. 1σ confidence intervals are given, apart from where the temperature or gravity of the object is beyond the range of the model grid and hence a χ^2 minimum has not been reached. Where a parameter is beyond the range of the model grid, the value is written in italics. The final columns show the total molecular hydrogen column density for each star, where it was detected and the measured interstellar extinction.

	BALMER LINE SPECTRA			LYMAN LINE SPECTRA				
Object	$T_{\rm eff}$ (K)	Log g	Log He/H	$T_{\rm eff}$ (K)	Log g	Log He/H	Log H_2	$E(B-V)$
A 7	66955 ± 3770	7.23 ± 0.17	−1.29 ± 0.15	99227 ± 2296	7.68 ± 0.06	−1.70 ± 0.09	18.5	0.001
HS 0505+0112	63227 ± 2088	7.30 ± 0.15	*−1.00*	*120000*	7.24	*−1.00*		0.047
PuWe 1	74218 ± 4829	7.02 ± 0.20	−2.39 ± 0.37	109150 ± 11812	7.57 ± 0.22	−2.59 ± 0.75	19.9	0.090
RE 0720−318	54011 ± 1596	7.68 ± 0.13	−2.61 ± 0.19	54060 ± 776	7.84 ± 0.03	−4.71 ± 0.69		0.019
TON 320	63735 ± 2755	7.27 ± 0.14	−2.45 ± 0.22	99007 ± 4027	7.26 ± 0.07	−2.00 ± 0.12	14.9	0.000
PG 0834+500	56470 ± 1651	6.99 ± 0.11	−2.41 ± 0.21	*120000*	7.19	*−5.00*	18.2	0.033
A 31	74726 ± 5979	6.95 ± 0.15	−1.50 ± 0.15	93887 ± 3153	7.43 ± 0.15	*−1.00*	18.8	0.045
HS 1136+6646	61787 ± 700	7.34 ± 0.07	−2.46 ± 0.08	*120000*	*6.50*	*−1.00*		0.001
Feige 55	53948 ± 671	6.95 ± 0.07	−2.72 ± 0.15	77514 ± 532	7.13 ± 0.02	−2.59 ± 0.05		0.023
PG 1210+533	46338 ± 647	7.80 ± 0.07	–	46226 ± 308	7.79±0.05	−1.03 ± 0.08		0.000
LB 2	60294±2570	7.60±0.17	−2.53 ± 0.25	87622±3717	6.96±0.04	−2.36 ± 0.17		0.004
HZ 34	75693±5359	6.51±0.04	−1.68 ± 0.23	87004± 5185	6.57±0.20	−1.73 ± 0.13	14.3	0.000
A 39	72451±6129	6.76±0.16	*−1.00*	87965±4701	7.06±0.15	−1.40 ± 0.14	19.9	0.130
RE 2013+400	47610±933	7.90±0.10	−2.80 ± 0.18	50487 ± 575	7.93±0.02	−4.02 ± 0.51		0.010
DeHt 5	57493±1612	7.08±0.16	−4.93 ± 0.85	59851±1611	6.75±0.10	*−5.00*	20.1	0.160
GD 561	64354±2909	6.94±0.16	−2.86 ± 0.35	75627±4953	6.64±0.06	−2.77 ± 0.24	19.8	0.089

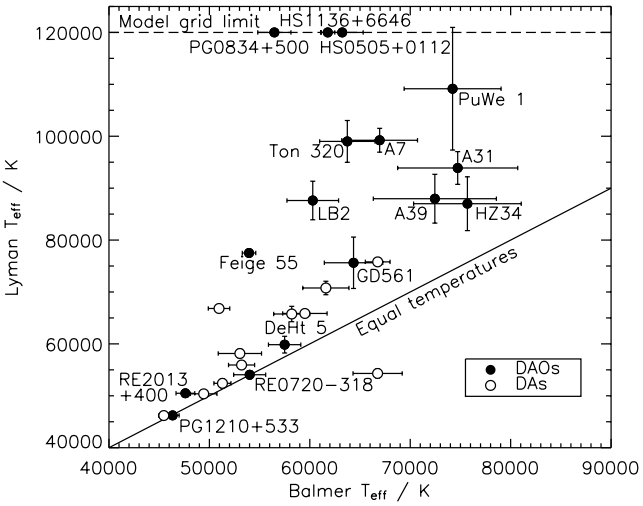

Figure 4. Scatter plot of the mean values of $T_{\rm eff}$ measured using ground-based Balmer and *FUSE* Lyman line data. The solid line corresponds to equal Balmer and Lyman line temperatures. For comparison, the results for DAs of Barstow et al. (2003b) are also shown.

in the DAO measurements than in the DAs, this might be because of the high H_2 absorption along the line of sight to a number of the DAOs and the underestimation of the true errors by the formal uncertainties. If this is not scatter, then some of the objects may form a second group, comprising the DAOs between Feige 55 and PuWe 1, incorporating LB 2, Ton 320 and A7, and extending to the DA RE 0457−281, which is one of the unusual objects identified by Barstow et al. This set of objects occupies a locus approximately parallel to the equal temperature line but their Lyman line $T_{\rm eff}$ values are displaced by a factor of ∼1.45 from the equal temperature line.

For three objects (HS 1136+6646, HS 0505+0112 and PG 0834+500), a model with temperature greater than the range of the model grid was required to reproduce the observed Lyman lines. By contrast, the Balmer line results place them in the middle of the range of temperatures seen for the DAOs in this sample. There is nothing obvious that relates these three objects, or the six that are described above, to each other, yet all seem to show a more extreme form of the Balmer/Lyman line discrepancy than the others. Note: HS 1136+6646 is a close double line spectroscopic binary with a K6 companion. A separate analysis of the Balmer and *FUSE* data of this star is contained in Sing et al. (2004). By subtracting a K star spectrum from the observed data before performing a fit to the Balmer lines using pure H, LTE models, they determined $T_{\rm eff}$ to be 70 000 K and log g to be 7.75. With this higher value for $T_{\rm eff}$, the temperature difference seems less extreme when compared to the other stars in the sample.

6.2 The Balmer line problem

The phenomenon of these Balmer/Lyman line temperature differences is similar in some ways to the Balmer line problem, because, in both, higher temperatures are required to fit certain lines. According to Napiwotzki (1999), if it is a lack of Stark broadened C, N and O in the models that is causing the Balmer line problem, a way of negating it is to fit only the higher order Balmer lines as these should yield temperatures closest to the 'true value'. Although statistically acceptable fits ($\chi^2_{\rm reduced} < 2$) are obtained in all our fits to the Balmer lines, to compare our results with those that use the Napiwotzki method to measure $T_{\rm eff}$ we re-analysed the optical spectra for three objects, but with only the δ, ϵ and He II 4686 Å lines used in the fit. If differences to the results of simultaneously fitting all lines are found, this also allows the strength of the two problems to be compared. The three re-analysed objects were chosen to encompass a range of strengths of the Balmer/Lyman temperature discrepancy problem. Table 3 lists the results. Fitting only the two higher order Balmer lines increases the statistical error on the temperature measurements by up to five to six times in some cases. Therefore, we compare the mean of the results for each observation, rather than the individual fits. For the first object, Ton 320, the new fit yields a temperature ∼15 000 K higher than the original analysis, but it is still ∼20 000 K cooler than the Lyman temperature. In the case of GD 561, fitting the higher order lines has produced a

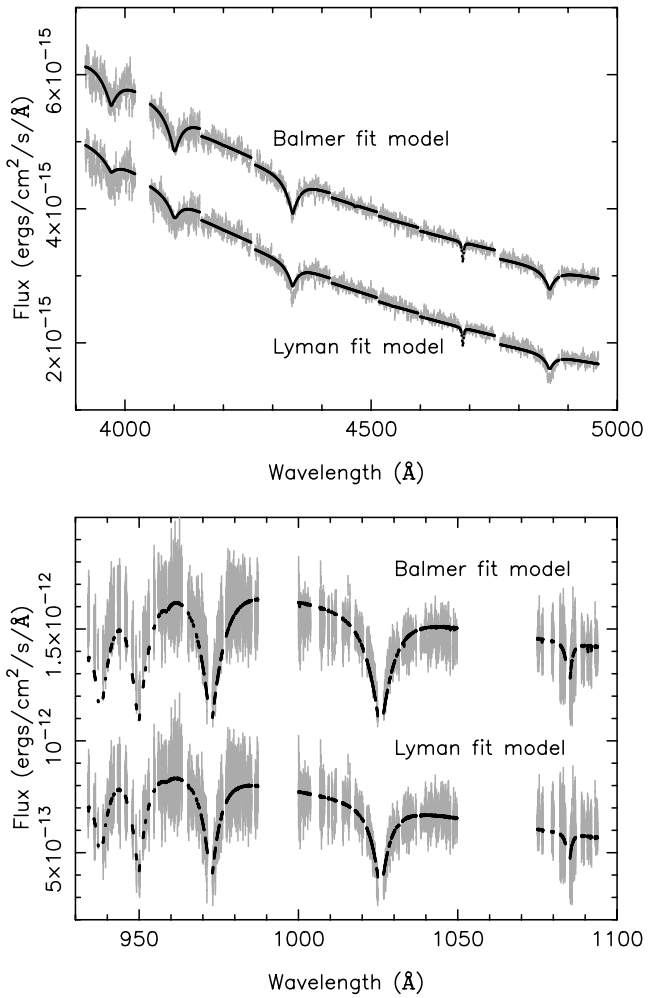

Figure 5. The optical and *FUSE* spectra of Ton 320 with the best-fitting models to the Balmer and Lyman lines overlaid. In both, the spectrum overlaid with the Balmer fit model has been shifted upwards for clarity. Because independent normalization constants are applied to each section of data in the fits to the optical spectra, slight discontinuities in the models can be seen.

temperature that agrees with the Lyman fit. However, the results are also in statistical agreement with the temperature determined using all the Balmer lines. RE 2013+400 is one of the objects where the Balmer and Lyman temperatures agree, but fitting only δ and ϵ lines decreases the temperature, and reduces the level of agreement. Therefore, as the temperatures measured using the Lyman lines were higher than those measured using the higher order Balmer lines in each case, we find that the original Balmer line problem does not appear to be related to our Balmer/Lyman line discrepency, nor is the Balmer line problem clearly manifest in any of the Balmer line spectra that were analysed (statistically acceptable fits were achieved for all). In addition, because of the increased uncertainties involved with fitting only the weak higher order Balmer lines, multiple observations are required to obtain reliable results for this method.

6.3 Surface gravity comparisons

Fig. 6 shows a scatter plot of the mean values of log g measured from the Balmer and Lyman line data. These measurements seem to agree well at high gravities, as was found by Barstow et al. (2003b). However, at lower gravities, considerable scatter is seen in the results. In a number of cases, the Lyman lines yield a lower gravity than the Balmer line measurements, but higher in others. This is as might be expected if the scatter is owing to random errors on the measurements, and hence there does not appear to be a trend of diverging log g at low gravities as suggested by Barstow et al. (2003b). The six objects that may exhibit a more extreme form of the temperature differences also do not show any systematic log g differences. The Lyman lines of the three objects that show the most extreme form of the problem are too weak and narrow to obtain meaningful measures of their gravities.

6.4 Helium abundance comparisons

A scatter plot of the Lyman and Balmer based helium abundances is shown in Fig. 7. The helium abundances agree closely for most of the objects studied, despite the model temperatures used in the Balmer and Lyman line wavelength regions differing greatly. Clearly the Balmer/Lyman temperature discrepency must be resolved before these results can be understood fully, but taken at face value, they imply that within the line-forming regions for the optical and *FUSE* wavelength ranges, the helium abundance remains approximately constant. However, there may be hidden systematic errors in the measurements because the helium abundance obtained from the *FUSE* data could be strongly influenced by the data-reduction and analysis techniques used, as the 1085 Å He II line falls within a noisy section of the combined spectra.

For two objects (RE 0720−318 and RE 2013+400), both of which are DAO+dM binaries, the helium abundances measured from *FUSE* data are significantly lower than that measured from the optical data. Dobbie et al. (1999) identified likely non-uniformities in the surface abundance of helium on RE 0720−318, which has a rotation period of 0.463 ± 0.004 d. This is consistent with models of accretion and hence the results may be showing a change in helium abundance with depth. However, to the first order, we would expect that helium abundance is homogeneous with depth in accretion models. Instead, if the surface abundance of helium is non-uniform or the accretion rate varying, the discrepancies may be owing to the different times at which the objects were observed in the two wavelength regions.

Table 3. Comparison of the best-fitting parameters to the Hδ and ϵ, and He II 4686 Å lines compared to fits to all the Balmer lines, and the temperature obtained from *FUSE* data.

	All Balmer lines and He			Hδ, ϵ and He only			*FUSE*
Object	$T_{\rm eff}$ (K)	Log g	Log He/H	$T_{\rm eff}$ (K)	Log g	Log He/H	$T_{\rm eff}$ (K)
Ton 320	63735±2755	7.27±0.14	−2.45 ± 0.22	78602±5996	7.28±0.11	−2.48 ± 0.10	99007±4027
RE 2013+400	47610±932	7.90±0.10	−2.80 ± 0.18	44994±2476	7.86±0.15	−2.27 ± 0.29	50487±575
GD 561	64354±2909	6.94±0.16	−2.86 ± 0.35	73350±5415	7.04±0.15	−2.58 ± 0.18	75627 ± 4953

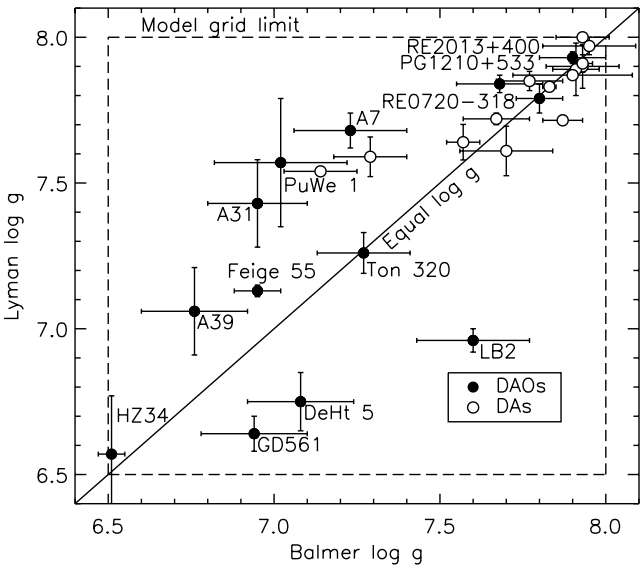

Figure 6. Scatter plot of the mean values of log g measured using ground-based Balmer and *FUSE* Lyman lines. The solid line corresponds to equal Balmer and Lyman line gravity. Results for HS 0505+0112, PG 0834+500 and HS 1136+6646 are not shown as a χ^2 minimum was not reached in the fit, and their Lyman lines are too weak and narrow to obtain reliable log g measurements. For comparison, the results for DAs of Barstow et al. (2003b) are also shown.

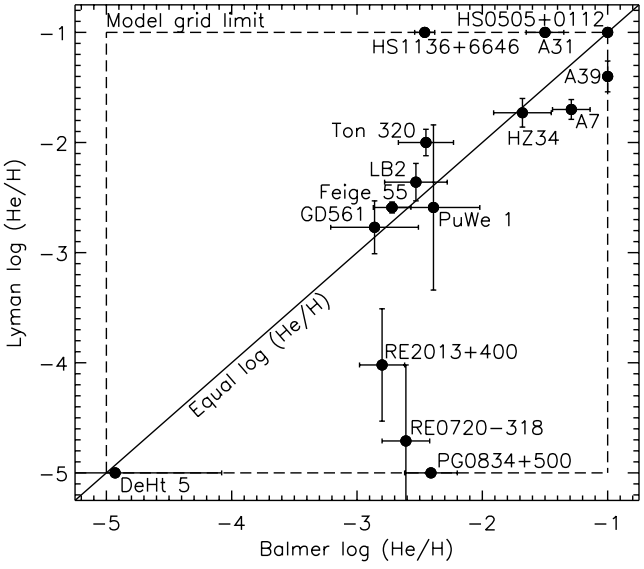

Figure 7. Scatter plot of the mean values of log $\frac{\mathrm{He}}{\mathrm{H}}$ measured from the strength of He II lines that lie within the wavelength ranges of the Balmer and Lyman line spectra. The solid line corresponds to equal abundances.

6.5 Correlation between parameters

A consideration when interpreting these results must be the correlation between parameters, as, for example, the models used to fit the Lyman lines of some of these white dwarfs are much hotter than those used to fit the Balmer lines, and this may affect the strength of the helium lines in the model spectra and consequently the helium abundance measurement. When performing a fit using XSPEC, a matrix of principle axes is output that indicates the correlation between parameters. No strong correlations between $T_{\rm eff}$, log g and log He/H were indicated by this. To further investigate potential correlations, the Balmer and Lyman line spectra of LB 2 were refitted but with the $T_{\rm eff}$, log g, or both, used in the fits fixed to the value obtained from the original fit to the data from the other wavelength region. LB 2 was chosen for this purpose as it is one of the objects for which differences are seen in both the temperature and gravity measurements, and the results of these fits are shown in Table 4. In fits to both the Balmer and the Lyman spectra, fixing $T_{\rm eff}$ to the Lyman and Balmer values, respectively, has resulted in the measured log g falling considerably. Similarly, fixing the log g values produces an increase in $T_{\rm eff}$ in both cases. However, this is perhaps not a valid comparison, because with the parameters fixed in this way, the line profiles are not reproduced as well by the models, resulting in an increase in the χ^2 statistic. By contrast, log He/H measured from the optical spectrum is not altered significantly by these changes to $T_{\rm eff}$ and log g, whereas that measured from the *FUSE* spectrum is decreased by forcing log g only, and both log g and $T_{\rm eff}$, to the Balmer line values. Setting $T_{\rm eff}$ alone to the Balmer fit value has resulted in an increase in the measured log He/H, although in this case log g has fallen to the limit of the model grid. Considering the differences in $T_{\rm eff}$ and log g measured from the Balmer and Lyman lines, the agreement in log He/H therefore seems surprising.

6.6 Dependence of differences on gravity and helium abundance

Fig. 8 illustrates the dependence of the temperature discrepancies between Balmer and Lyman measurements on gravity. The differences appear to be smallest at the edges of the log g range. At high log g are RE 0720−318, RE 2013+500 and PG 1210+533, which are the DAOs that most resemble DAs in their temperatures and gravities and hence are relatively cool and high gravity compared to the other DAOs. As the temperature differences are smallest at low temperatures, it is unsurprising that there is an apparent minimum in temperature difference at high gravity.

For the remaining objects, the temperature discrepancies appear to decrease at lower gravities, although there is considerable scatter on the measurements. As a white dwarf cools, its surface gravity increases (see Fig. 9), hence, in general, the hottest white dwarfs should have the lowest surface gravities. Therefore, as the hottest white dwarfs exhibit the largest temperature differences, it might be expected that the lowest log g objects also have the largest discrepancies, which is the opposite to the trend seen. This could point to an effect that would be expected to have a dependence on gravity, such as stratification driven by radiative acceleration, or mass loss, causing the Balmer/Lyman temperature problem.

As both stratification and mass loss are radiatively driven effects, the temperature differences might show a dependence on the luminosity of the star. By combining the $T_{\rm eff}$ and log g measurements with the evolutionary models of Bloecker (1995) and Driebe et al. (1998), the luminosity of each white dwarf was determined. These are plotted against the temperature discrepancies in Fig. 10, and show that the differences are greatest at high luminosities. The luminosity of a white dwarf should increase with temperature but fall with increased gravity; therefore the observed decrease in temperature difference towards low gravity is contrary to what might be expected if the stratification of white dwarf atmospheres is causing these differences. However, the real issue is how the temperature of the best-fitting homogeneous model compares with the real effective temperature of a white dwarf whose atmosphere is stratified. In radiative levitation models (e.g. Chayer, Fontaine, & Wesemael 1995) changing log g alters the distribution of elements within the model

Table 4. Effect on the best-fitting parameters to the spectra of LB 2 when $T_{\rm eff}$ or log g, or both, in the model fit to the Balmer or Lyman lines are fixed at the value obtained from fitting the data from the other wavelength region. Values that were fixed are shown in bold, and where a parameter is beyond the range of the model grid, the value is written in italics and no errors are calculated.

	BALMER LINE SPECTRUM			*FUSE* SPECTRUM		
	$T_{\rm eff}$ (K)	Log g	Log He/H	$T_{\rm eff}$ (K)	Log g	Log He/H
Best-fitting parameters	60294±2570	7.60±0.17	−2.53 ± 0.25	87622±3717	6.96±0.04	−2.36 ± 0.17
$T_{\rm eff}$ fixed	**87622**	6.70±0.12	−2.49 ± 0.32	**60294**	*6.50*	−2.67
Log g fixed	66077±2444	**6.96**	−2.47 ± 0.25	99537±1208	**7.60**	−2.00 ± 0.03
$T_{\rm eff}$ and log g fixed	**87622**	**6.96**	−2.53±0.17	**60294**	**7.60**	−1.09 ± 0.02

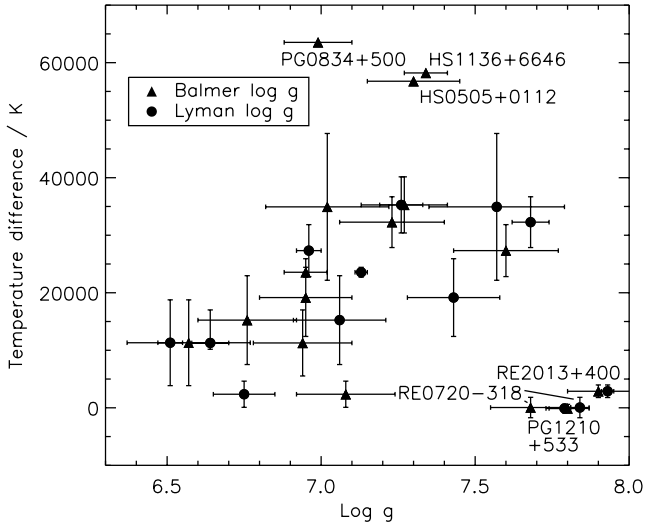

Figure 8. Dependence of temperature difference (Lyman temperature minus Balmer temperature) on log g.

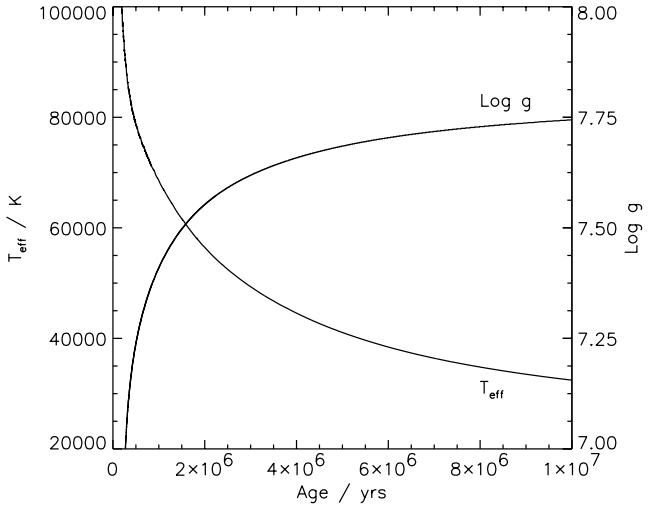

Figure 9. The $T_{\rm eff}$ and log g of a 0.530 $M_{\odot}$ white dwarf as it cools, according to the models of Bloecker (1995). As the Balmer/Lyman temperature differences increase with temperature, it might be expected that they would also be largest in the lowest gravity stars.

white dwarf atmosphere; therefore, it is possible that homogeneous models are a better approximation to reality at low gravity, resulting in better agreement between optical and far-UV temperatures. A comparison of homogeneous models with the self-consistent non-

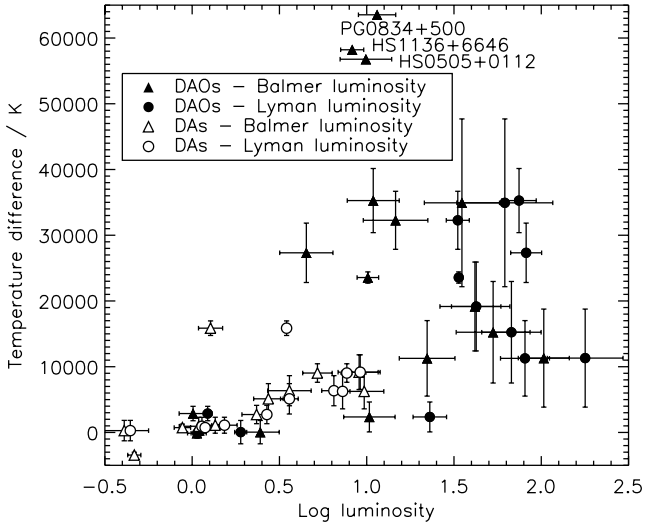

Figure 10. The dependence of the temperature differences (Lyman temperature minus Balmer temperature) on the luminosity of the objects. Luminosities were determined by combining the evolutionary models of Bloecker (1995) and Driebe et al. (1998) with the measured $T_{\rm eff}$ and log g of an object; these are referred to as Balmer luminosities if the temperature and gravity used were obtained from fitting the Balmer lines, Lyman luminosities if the Lyman line fit was used. For comparison, the results for DAs of Barstow et al. (2003b) are also shown.

chemically homogeneous models that are currently being developed (e.g. Schuh, Dreizler & Wolff 2002), and with models incorporating mass loss, is required to determine if they show the observed trends with log g and $T_{\rm eff}$.

A similar comparison with helium abundance is shown in Fig. 11. Although the temperature discrepancies appear lower when the helium abundance is also low, this result is biased by the low log He/H obtained from the *FUSE* data for the two DAO+dM binaries. As the objects analysed by Barstow et al. (2003b) all have low helium abundance (because they are DAs), yet still exhibit Balmer/Lyman line temperature discrepancies, it does not appear likely that these differences are related to the presence of helium in the white dwarf atmosphere to the first order.

7 CONCLUSION

$T_{\rm eff}$, log g and log He/H have been determined for a sample of 16 DAO white dwarfs using Balmer and Lyman line spectra. The divergence of Lyman and Balmer line derived measurements of $T_{\rm eff}$ at temperatures above 50 000 K has been found to continue in stars hotter than 70 000 K. The problem appears to be present in slightly greater strength in six of the objects, although the size

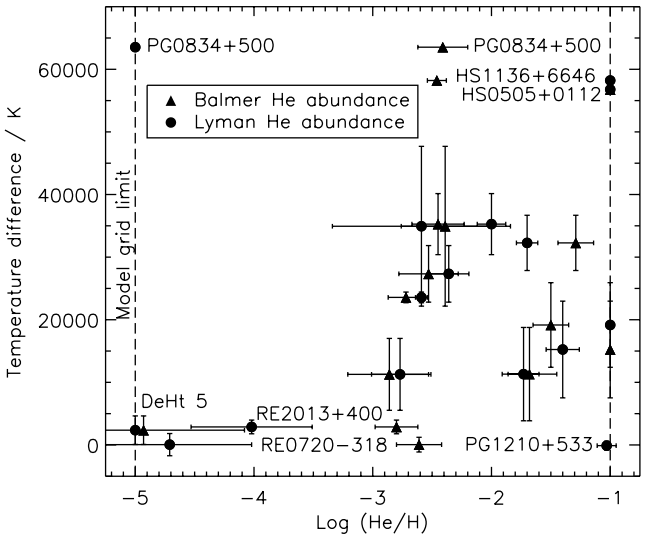

Figure 11. Dependence of temperature difference (Lyman temperature minus Balmer temperature) on log He/H.

of the measurement errors may be sufficient to explain these by random scatter. A comparison was made with the strength of the Balmer line problem, which can affect measurements of $T_{\rm eff}$ of both DAs and DAOs. None of the objects studied were found to be strongly affected by the problem, and by comparing the temperatures obtained from fitting only the higher order Balmer lines, the Balmer line problem was found to be a weaker effect than the Balmer/Lyman line discrepancies. A further three objects exhibited an extreme form of the problem. For these stars the Lyman lines are so weak that they could not be fitted using our model grid.

Systematic differences between Balmer and Lyman line gravity measurements were not found. At higher gravity ($\log g > 7.7$), agreement between the Balmer and Lyman line measurements was good, although at lower gravities there was considerable scatter in the measurements. The measurements of helium abundance agreed well between the two wavelength regions, even though the temperatures of the best-fitting models varied a great deal. Two DAO+dM binaries were exceptions, with the helium abundances measured from *FUSE* data lower than that measured from Balmer line data. These close binaries have rotation periods of order a day, so surface inhomogeneities may account for the variable He abundance measurements, as the stars may have been observed at different phases in the optical and far-UV. Alternatively, if the white dwarf were experiencing periods of increased or decreased accretion rate, this could also account for the observed differences.

Full interpretation of the helium abundances measured using data from the two wavelength regimes must be reserved until the cause of the Balmer/Lyman discrepancies are known and uncertainties in the model temperature and gravity that should be used to fit the data are resolved. As the temperature discrepancies seem reduced in stars with lower surface gravity and luminosity, work on overcoming this problem might focus initially on effects such as the stratification of elements in the white dwarf atmosphere, and mass loss.

ACKNOWLEDGMENTS

The authors would like to thank Pierre Bergeron for allowing the use of his data for this work and for his comments. Based on observations made with the NASA–CNES–CSA Far Ultraviolet Spectroscopic Explorer. *FUSE* is operated for NASA by the Johns Hopkins University under NASA contract No. NAS5-32985. Also based on observations made using the Steward Observatory, Arizona, USA. SAG, MAB, MRB and PDD were supported by PPARC, UK; MRB acknowledges the support of a PPARC Advanced Fellowship. JBH and DKS wish to acknowledge support from NASA grant Nos NAG5-10700 and NAG5-13213.

REFERENCES

Arnaud K. A., 1996, in Jacoby G H., Barnes J., eds, ASP Conf. Ser. Vol. 101, Astronomical Data Analysis Software and Systems V. Astron. Soc. Pac., San Francisco, p. 17
Barstow M. A. et al., 1994a, MNRAS, 271, 175
Barstow M. A., Holberg J. B., Fleming T. A., Marsh M. C., Koester D., Wonnacott D., 1994b, MNRAS, 270, 499
Barstow M. A., Hubeny I., Holberg J. B., 1998, MNRAS, 299, 520
Barstow M. A., Bannister N. P., Holberg J. B., Hubeny I., Bruhweiler F. C., Napiwotzki R., 2001a, MNRAS, 325, 1149
Barstow M. A., Holberg J. B., Hubeny I., Good S. A., Levan A. J., Meru F., 2001b, MNRAS, 328, 211
Barstow M. A., Good S. A., Holberg J. B., Hubeny I., Bannister N. P., Bruhweiler F. C., Burleigh M. R., Napiwotzki R., 2003a, MNRAS, 341, 870
Barstow M. A., Good S. A., Burleigh M. R., Hubeny I., Holberg J. B., Levan A. J., 2003b, MNRAS, 344, 562
Bergeron P., Saffer R. A., Liebert J., 1992, ApJ, 394, 228
Bergeron P., Wesemael F., Beauchamp A., Wood M. A., Lamontagne R., Fontaine G., Liebert J., 1994, ApJ, 432, 305
Bloecker T., 1995, A&A, 297, 727
Chayer P., Fontaine G., Wesemael F., 1995, ApJS, 99, 189
Dobbie P. D., Barstow M. A., Burleigh M. R., Hubeny I., 1999, A&A, 346, 163
Driebe T., Schoenberner D., Bloecker T., Herwig F., 1998, A&A, 339, 123
Holberg J. B., Wesemael F., Wegner G., Bruhweiler F. C., 1985, ApJ, 293, 294
Hubeny I., Lanz T., 1995, ApJ, 439, 875
Koester D., Weidemann V., Schulz H., 1979, A&A, 76, 262
McCandliss S. R., 2003, PASP, 115, 651
Moos H. W. et al., 2000, ApJ, 538, L1
Napiwotzki R., 1999, A&A, 350, 101
Napiwotzki R., Schöberner D., 1993, in Barstow M., ed., 8th European Workshop on White Dwarfs. Kluwer Academic Publishers, Dordrecht, p. 99
Sahnow D. J. et al., 2000, ApJ, 538, L7
Schuh S. L., Dreizler S., Wolff B., 2002, A&A, 382, 164
Seaton M. J., 1979, MNRAS, 187, 73P
Sing D. K. et al., 2004, AJ, 127, 2936
Unglaub K., Bues I., 1998, A&A, 338, 75
Unglaub K., Bues I., 2000, A&A, 359, 1042
Vennes S., Pelletier C., Fontaine G., Wesemael F., 1988, ApJ, 331, 876
Werner K., 1996, ApJ, 457, L39
Wesemael F., Greenstein J. L., Liebert J., Lamontagne R., Fontaine G., Bergeron P., Glaspey J. W., 1993, PASP, 105, 761

This paper has been typeset from a TEX/LATEX file prepared by the author.